Journal of Sustainable Cement-Based Materials

ISSN: (Print) (Online) Journal homepage: https://www.tandfonline.com/loi/tscm20

Poly(aspartic acid) superabsorbent polymers as biobased and biodegradable additives for self-sealing of cementitious mortar

Lauren De Grave, José Roberto Tenório Filho, Didier Snoeck, Sofiya Vynnytska, Nele De Belie, Katrien V. Bernaerts & Sandra Van Vlierberghe

To cite this article: Lauren De Grave, José Roberto Tenório Filho, Didier Snoeck, Sofiya Vynnytska, Nele De Belie, Katrien V. Bernaerts & Sandra Van Vlierberghe (2022): Poly(aspartic acid) superabsorbent polymers as biobased and biodegradable additives for self-sealing of cementitious mortar, Journal of Sustainable Cement-Based Materials, DOI: 10.1080/21650373.2022.2137861

To link to this article: https://doi.org/10.1080/21650373.2022.2137861

Published online: 27 Oct 2022.

Journal of Sustainable Cement-Based Materials, 2022
http://dx.doi.org/10.1080/21650373.2022.2137861

Poly(aspartic acid) superabsorbent polymers as biobased and biodegradable additives for self-sealing of cementitious mortar

Lauren De Grave[a,b], José Roberto Tenório Filho[c], Didier Snoeck[d], Sofiya Vynnytska[a,b], Nele De Belie[c], Katrien V. Bernaerts[b] and Sandra Van Vlierberghe[a]*

[a]*Polymer Chemistry and Biomaterials Group (PBM), Centre of Macromolecular Chemistry, Department of Organic and Macromolecular Chemistry, Ghent University, Ghent, Belgium;* [b]*Aachen-Maastricht Institute for Biobased Materials (AMIBM), Brightlands Chemelot Campus, Maastricht University, Geleen, The Netherlands;* [c]*Magnel-Vandepitte Laboratory, Department of Structural Engineering and Building Materials, Ghent University, Ghent, Belgium;* [d]*Building, Architecture and Town Planning (BATir) Department, Université Libre de Bruxelles (ULB), Brussels, Belgium*

Concrete is currently the most used man-made construction material. Unfortunately it is prone to defects, such as cracks. Crack repair is possible by incorporation of superabsorbent polymers (SAPs) which can fill a crack by swelling and promote formation of healing products. However, SAPs are usually acrylate-based and not biodegradable. Present work focuses on development of SAPs based on poly(aspartic acid) (PASP), which is a biobased and biodegradable alternative of acrylate-based polymers. The developed SAP was incorporated in mortar and the effect on the mortar properties was studied. When adding 1 m% SAP, a decrease in strength was observed, similar to commercially available acrylate-based SAPs. The SAPs showed an efficient and immediate sealing effect in cracked mortar, reflected by a reduction in water permeability over 50%. Hence, the developed biobased SAP shows good sealing properties and could be used as a sustainable alternative for acrylic SAPs in concrete repair.

Keywords: poly(aspartic acid); superabsorbent polymers; sustainable; cementitious materials; self-sealing

1. Introduction

Superabsorbent polymers (SAPs) are slightly crosslinked hydrogels consisting of water-soluble polymers, most frequently composed of ionic monomers. As a result of their limited crosslink density, combined with their intrinsic hydrophilicity, they have the ability to absorb and retain aqueous solutions up to several hundred times their own weight with retention of their original shape [1–3]. SAPs with an absorption capacity of $10-1000\,g\ g^{-1}$ have already been reported, while common hydrogels have an absorption capacity of about $1\,g\ g^{-1}$ [4]. Furthermore, they have the ability to retain the absorbed water upon heating or exposure to pressure. Because of their unique properties, SAPs find their application in several fields in which their extraordinary swelling capacity is an asset, such as disposable diapers and other hygiene products [5,6], biomedical applications (*e.g.* controlled drug release and wound healing) [5,7,8], water purification systems [9] and agriculture (*e.g.* soil stabilizers, nutrient carriers, controlled release of pesticides and water reservoirs) [10–15]. Some SAPs can also be applied as 'smart' polymers that undergo remarkable changes in swelling capacity upon small environmental changes like pH, temperature, light and pressure [16], which renders them especially useful in the field of controlled drug release [7,17,18]. Another application that gained a lot of attention in recent years is the use of SAPs as additive in cementitious materials [2,3].

SAPs can be subdivided into two main classes, namely synthetic or chemical SAPs and natural SAPs based on polysaccharides or polypeptides. Synthetic SAPs, which are mainly based on acrylates and acrylamides, are the largest class and currently the most frequently used as a result of their high water-solubility and polyanionic character. However, acrylates are derived from petrochemicals and are non-biodegradable, imposing a major burden to the environment [19]. Also, since crude oil is finite and becomes more expensive, the use of synthetic acrylate-based SAPs will become less profitable [16]. Even though research regarding natural alternatives has been emerging in recent years and several articles on natural SAPs, derived from polysaccharides (*e.g.* starch, cellulose, chitosan, alginate, *etc.*) [19] and polypeptides (*e.g.* soy-protein, fish-protein, poly(glutamic acid), *etc.*) [20] have been published, synthetic SAPs still have the largest market share to date [21]. Therefore, the search for more environmentally friendly alternatives remains important.

An interesting type of polymer that has been recognized as an excellent alternative to replace poly(acrylic acid) and other acrylate-based polymers is poly(aspartic acid) (PASP). Similar to poly(acrylic acid), it is a water-soluble polymer with polyanionic character in neutral medium resulting in a high swelling capacity when crosslinked [22,23]. The starting monomer is aspartic acid, which is an amino acid, resulting in a biobased polymer. Since PASP is a polypeptide, it is also biodegradable in

*CONTACT Sandra Van Vlierberghe Sandra.VanVlierberghe@UGent.be Polymer Chemistry and Biomaterials Group (PBM), Centre of Macromolecular Chemistry, Department of Organic and Macromolecular Chemistry, Ghent University, Ghent, Belgium
Supplemental data for this article can be accessed online at https://doi.org/10.1080/21650373.2022.2137861.

Table 1. Summary of the most important characteristics of commercial SAPs A and B used for comparison with the synthetic SAP; values obtained from [77].

	SAP A	SAP B
Constitution	copolymer of acrylamide and sodium acrylate	crosslinked potassium salt poly(acrylate)
Nominal particle size (μm)	100.0 ± 21.5	476.6 ± 52.9
Moisture uptake capacity (%) (RH 60%/90%/98%)	26/83/394	28/84/394
Sorption capacity in DDW (g g^{-1})	305.0 ± 3.7	283.2 ± 2.4
Sorption capacity in CF (g g^{-1})	61.0 ± 1.0	58.4 ± 1.7
Additional water added during mixing (g g^{-1})	30.5	8.9
Reduction tensile strength (%) (SAP content 0.5 m%/1 m%)	−1/14	−4/0
Reduction compressive strength (%) (SAP content 0.5 m%/1 m%)	36/56	22/22

physiological and environmental conditions, *e.g.* in activated sludge, in river water by microbial degradation and in environments containing several types of enzymes, and it will only release non-toxic natural compounds upon degradation [24,25]. Furthermore, synthesis of PASP is rather straightforward and the polymer precursor, polysuccinimide (PSI), easily reacts with primary amines under mild reaction conditions giving access to a broad range of possible side-groups [26]. PASP is usually modified with diamines, poly(ethylene glycol)-diepoxide or aminothiols like cysteamine that can be crosslinked, resulting in PASP-based hydrogels and SAPs [27]. Hydrogels and SAPs based on PASP have been reported in a plethora of applications, especially in the biomedical field as a result of their biocompatibility [28], *e.g.* scaffolds for tissue engineering [29–31], coatings to prevent biofouling [32], carriers for DNA and RNA transfection [33–36], 'smart' hydrogels for controlled drug release [37–41], *etc.* Other reported applications involving PASP-based SAPs include sand-fixing agents [42], water-retaining agents [43] and fertilizers [44]. Surprisingly, to the best of our knowledge, no study has been reported on the usage of PASP-based SAPs to support self-healing in concrete.

SAPs have been widely investigated in concrete to provide internal curing and to reduce autogenous shrinkage [45–48]. Additionally, they were found to promote (immediate) sealing of cracks [49–53] and to enhance self-healing [54–56]. Concrete is worldwide the most used man-made construction material, but a downside is the sensitivity of the material to cracks as a result of a limited tensile strength. In most cases, concrete is reinforced with steel to carry the tensile load, but, even with steel reinforcement, cracks are not completely excluded and form a threat to the durability of the material when the reinforcement is corroded by liquids and gasses penetrating the crack. Several methods for crack repair exist [57–59], but these are generally expensive, time-consuming, visually impairing and sometimes impossible to use when the crack is formed at inaccessible places. In this regard, methods for crack repair could highly benefit from the autogenous healing of concrete [60] or some immediate self-sealing mechanism. Autogenous healing in concrete can be a result of further hydration of non-hydrated cement particles with formation of calcium silicate hydrates (C–S–H) and/or carbonation of $Ca(OH)_2$ resulting in formation and precipitation of $CaCO_3$, which causes cracks to heal [61,62]. However, autogenous healing can only heal small cracks (complete healing of cracks up to 50 μm and partial healing of cracks $\leq$150 μm) and is only possible when water is present, which strongly depends on the outer environment of the concrete [16,54,63,64]. Several methods exist to promote autogenous healing and subsequent crack repair [65], including the incorporation of SAPs. On the one hand, SAPs have a direct sealing effect by swelling when water is penetrating the crack, preventing further water ingression [49]. On the other hand, SAPs can serve as a water reservoir providing their absorbed moisture during dry periods, resulting in a more continuous water supply for autogenous healing [54]. Since the first reports on SAPs for cementitious materials in the late 1990s and early 2000s [45,66,67], these materials have been the subject of many studies, which are summarized in recent reviews covering the different aspects and versatile actions of SAPs in concrete [2,3]. The majority of SAPs used for concrete applications are acrylate-based, but also non-acrylic SAPs were specifically designed for application in cementitious materials [52,68,69]. Also, several recent reports have been published on the use of biopolymers as SAPs to introduce self-healing and to mitigate shrinkage [70–76], However, despite all efforts and research that has been conducted, more environmentally friendly alternatives for acrylate-based SAPs remain relatively scarce.

Therefore, we aim to select a new type of biobased polymer to create SAPs for concrete repair. In the present work, the potential of PASP-based SAPs to support self-sealing and self-healing of cracks is investigated. To this end, a novel type of modified PASP was synthesized and characterized for chemical structure verification through nuclear magnetic resonance (^{1}H-NMR) spectroscopy, gel permeation chromatography (GPC) and *in situ* photo-rheology. Afterwards, the modified PASP was crosslinked to obtain a SAP. The water absorption capacity was first studied through swelling experiments and dynamic vapor sorption (DVS) measurements. The SAP was dried and ground to powder and mixed into mortar, after which the effect on the microstructure and mechanical properties were studied. Results were compared with two widespread commercial acrylate-based SAPs, namely SAP A, a copolymer of acrylamide and sodium acrylate and SAP

B, a crosslinked potassium salt poly(acrylate) [77]. The most important characteristics of the commercial SAPs that are used for comparison are summarized in Table 1. Finally, the self-sealing and self-healing properties of the material were assessed by means of water permeability tests on cracked mortar specimens before and after healing cycles.

2. Materials and methods

2.1. Materials

All chemicals were used as received unless stated otherwise. *L*-aspartic acid was purchased from Th. Geyer. *o*-Phosphoric acid (H_3PO_4, cryst., 99%) and N,N-dimethylformamide (DMF, >99.9%) were obtained from VWR. Methanol (MeOH, >99%) was purchased from Chem-Lab. Sodium hydroxide (NaOH, pellets) and DL-dithiothreitol (DTT, 97%) were purchased from Sigma-Aldrich. 5-Norbornene-2-methylamine (mixture of isomers, >98%) was acquired from TCI Europe. Deuterated dimethylsulfoxide (*d6*-DMSO, 99.8% D) and deuterium oxide (D_2O, 99.9% D) were obtained from Eurisotop. Ethyl acetate was supplied by UnivarSolutions. Lithium (2,4,6-trimethylbenzoyl)phenylphosphinate (Li-TPO-L) was prepared according to a procedure reported by Markovic *et al.* [78]. Dialysis membranes Spectra/Por (MWCO 3500 g mol^{-1}) were purchased from Polylab. Double distilled water (DDW) was used for preparation of aqueous solutions and swelling experiments (Merck Synergy UV, Millipore Milli-Q gradient, $\rho = 18.2$ MΩ cm at 25 °C).

2.2. Synthesis of polysuccinimide and modification to obtain norbornene-modified poly(aspartic acid)

Polysuccinimide (PSI) was synthesized according to a modified procedure described by Zrinyi *et al.* [79]. 65.10 g (0.49 mol) *L*-aspartic acid and 65.06 g (0.66 mol) crystalline H_3PO_4 were mixed in a round-bottom flask and heated to 180 °C under vacuum with a rotary evaporator. The vacuum was maintained at 10 mbar for 7 h to obtain a light-brown viscous product. This product was dissolved overnight in 650 mL DMF by stirring and heating to 70 °C. Purification was done by precipitation in methanol (10-fold excess compared to the DMF used), followed by filtration and washing with an alkaline solution (aq. NaOH solution, pH 9) until the washing water became neutral. The resulting product was dried for 4 days in vacuum at 50 °C. PSI was obtained as a white solid in 94% yield.

Norbornene-modified poly(aspartic acid) (PASP-NB) was obtained *via* modification of PSI with 5-norbornene-2-methylamine (NB-NH_2) according a procedure described in literature [80], followed by hydrolysis and dialysis of the intermediate. 20.00 g PSI (0.21 mol succinimide units) was dissolved in 200 mL DMF in a flame-dried two-neck flask while stirring and heating to 60 °C. After complete dissolution, 0.20 eq. (relative to the amount of succinimide units) NB-NH_2 (0.04 mol, 5.07 g, 5.07 mL) was added to the PSI solution. The system was filled with Argon gas and degassed 3 times. The reaction was continued for 24 h at 60 °C. Afterwards, the polymer was precipitated by addition of the reaction solution to ethyl acetate (12-fold excess compared to the DMF used), followed by filtration and washing 3 times with ethyl acetate. The precipitate was dried under vacuum at room temperature for 48 h to obtain norbornene-modified PSI (PSI-NB) as intermediate product. PSI-NB was dispersed in DDW with a concentration of 10 w/v%. The pH of the solution was adjusted to 10 by adding 1 M NaOH solution dropwise to the suspension in order to hydrolyze the succinimide units. The reaction mixture was stirred for 3 h while regularly checking the pH and readjusting to pH 10 if necessary. The solution was dialyzed against DDW (Spectra/Por MWCO 3500 g mol^{-1}) for 24 h with the water being changed 6 times. Finally, PASP-NB was obtained after freezing and lyophilization (Christ freeze-dryer Alpha 2-4 LSC). PASP-NB was obtained as white/yellow fine powder with an overall yield of 98%.

2.3. Polymer characterization

2.3.1. Nuclear magnetic resonance (^{1}H-NMR) spectroscopy

All ^{1}H-NMR spectra were recorded using a 300 MHz Bruker Avance I Ultrashield spectrometer at room temperature with *d6*-DMSO or D_2O as solvent. Spectra were analyzed using MestReNova software.

2.3.2. Gel permeation chromatography (GPC)

Gel permeation chromatography (GPC) was performed on a Waters Alliance e2696 Separations Module device coupled to a Styragel Guard Column (4.6 × 30 mm, packed with 20 µm particles) and three Styragel GPC Columns (7.8 × 300 mm, packed with 5 µm particles) with variable molecular weight range ($0 - 1000$ g mol^{-1}, $500 - 20000$ g mol^{-1} and $5000 - 600000$ g mol^{-1}) connected in sequence with a column temperature of 40 °C. Detection was based on a refractive index (RI) detector 2414 with RID temperature 35 °C. Molar masses were determined from the obtained retention times *via* an external calibration curve using ReadyCal-Kit PMMA standards ($M_p = 800 - 2200000$ g mol^{-1}). As eluent DMF + 0.035 mol L^{-1} LiCl + 6 mol L^{-1} glacial acetic acid was used at a flow rate of 1 mL min^{-1}. Samples were prepared by dissolving $2 - 5$ mg of polymer in 1.5 mL of the eluent.

2.3.3. Photo-rheology

Photo-rheology measurements were carried out on an Anton Paar Physica MCR 301 rheometer with plate-plate geometry, with upper plate diameter being 25 mm. All measurements were performed at 20 °C with an oscillatory frequency of 1 Hz, a strain of 0.1% and a measuring gap of 0.25 mm. 300 µL of the sample was injected between the parallel plates, the samples were trimmed and irradiated through a quartz glass bottom plate using UV-A light with a wavelength of 365 nm and an intensity of 3500 mW cm^{-2} (EXFO Novacure 2100 UV light source). Samples were irradiated for 600 s, samples were not

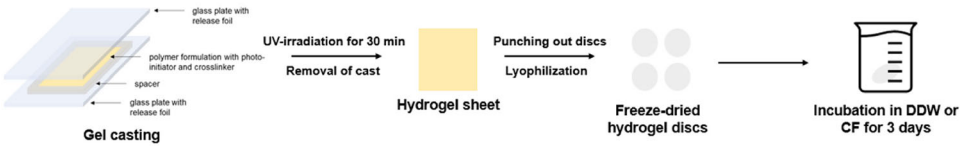

Figure 1. Schematic representation of the production of hydrogel sheets *via* gel casting, followed by punching out of circular samples, lyophilization and start of the swelling experiments.

irradiated for 60 s before and after UV curing. All samples were crosslinked at 20 w/v% PASP-NB concentration in DDW in the presence of 2 mol% Li-TPO-L as photo-initiator, relative to the number of crosslinkable functionalities present in the polymer. 0.50 eq. DTT, relative to the number of crosslinkable functionalities, was added as crosslinker corresponding to an equimolar thiol-ene ratio allowing efficient crosslinking.

2.4. Hydrogel formation hydrogels

For the formation of crosslinked hydrogels, a 20 w/v% solution of PASP-NB was prepared in DDW at room temperature. After complete dissolution, 2 mol% Li-TPO-L and 0.50 eq. DTT (both relative to the number of crosslinkable functionalities present) were added. The solution was injected between two parallel quartz glass plates with Teflon release foil and a silicone spacer of 1 mm thickness. The plates were irradiated on both sides with UV-A light (365 nm, UVP High Performance UV Transilluminator) with intensity 10 mW cm^{-2} for 30 min to induce crosslinking of the solution. After irradiation, the plates were removed from each other to release the crosslinked hydrogel sheet. For determination of swelling and gel fraction, discs (Ø = 8 mm) were punched out from the sheet, which were then frozen and lyophilized. For preparation of the SAP powder, the sheets were first frozen and lyophilized, followed by grinding and sieving.

2.5. Dynamic vapor sorption (DVS) measurements

Dynamic vapor sorption (DVS) measurements were carried out to determine the moisture uptake capacity of the material at different relative humidities (RH) and the hysteresis of the sample upon desorption. The DVS device consists of a Cahn microbalance, a temperature-controlled housing and mass flow controllers to control the flow of wet and dry N_2 gas. This set-up allows to control both RH and temperature. For these measurements, the temperature was set at 20 °C. 10 mg freeze-dried SAP powder was placed in the sample pan. A first step of RH 0% was established to start with completely dry material. Afterwards, the RH was increased in systematic steps of 10%, with a final step of 8%, until a RH of 98% was reached. Every subsequent step was initiated when the change in sample mass as a function of time was lower than 0.002 mg min^{-1}. After an equilibrium value was obtained at the highest RH, desorption was realized by decreasing the RH in the same systematic steps as the sorption process until full desorption was realized.

2.6. Swelling studies in water and cement filtrate solution

Swelling and gel fraction experiments were carried out in water using 8 mm hydrogel discs that were punched out of a crosslinked hydrogel sheet (see section 2.4) with a thickness of 1 mm. The obtained samples were first frozen and lyophilized to start with an initial dry mass. Because the hydrogel discs were expected to swell to a high extent, the discs were placed in histology cassettes to avoid loss of material. Afterwards, samples were incubated in DDW for 3 days at 20 °C, followed by freezing and lyophilization. A schematic representation of the process is shown in Figure 1. The swelling ratio and gel fraction were calculated according to equation (Eq. 1) and (2) respectively:

$$\text{Swelling ratio} = \frac{m_s - m_{d,2}}{m_{d,2}} \quad (1)$$

$$\text{Gel fraction (GF)} = \frac{m_{d,2}}{m_{d,1}} \times 100\% \quad (2)$$

$m_{d,1}$ is the initial freeze-dried mass of the sample before swelling, $m_{d,2}$ is the final freeze-dried mass of the sample after swelling and m_s is the mass of the sample in swollen state. All measurements were performed in triplicate for statistical relevance.

The sorption capacity of the SAP powder was determined *via* a filtration method as described in RILEM TC 260-RSC [81]. Approximately 20 mg of SAP powder was incubated in DDW for 24 h at 20 °C. The SAP was filtered over a filter that was saturated with fresh test solution to avoid influence of the paper and a lid was added on top of the filter to avoid influences of evaporation. The mass of the filtrate was recorded and the powder was again lyophilized. The sorption capacity was calculated according to Eq. (3):

$$\text{Sorption capacity} = \frac{m_2 - m_3}{m_1} \quad (3)$$

m_1 is the final freeze-dried mass of the powder after swelling, m_2 is the original mass of the test solution before the experiment and m_3 is the mass of the filtrate obtained after the experiment. All measurements were performed in triplicate for statistical relevance.

Also the sorption capacity in cement filtrate (CF) solution was determined. CF was prepared by mixing 10 g Portland cement (CEM I 52.5 N) and 100 mL demineralized water for 24 h with a mechanical stirrer. Afterwards, the suspension was filtered to remove the cement particles and to obtain a solution with a similar composition as the pore solution to which the SAP will be exposed during preparation of the concrete. Care was taken to avoid carbonation of the liquid by shielding the suspension from air with aluminum foil during mixing and filtering. The

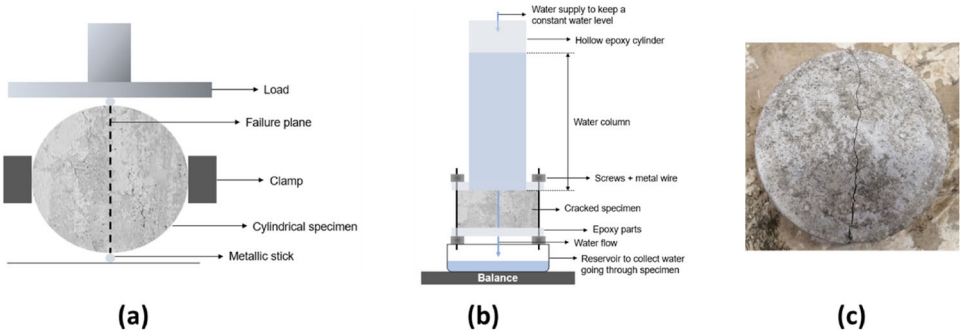

Figure 2. Schematic representation of (a) the splitting tensile test method to create the cracked specimens (based on [84]) and (b) the constant-head test set-up (based on [85]), (c) image of a cracked specimen.

sorption capacity was measured both for the hydrogel discs and the SAP powder as described before, only replacing DDW with CF. The sorption capacities were calculated *via* Eq. (1) and (3).

2.7. Infrared spectroscopy on dried hydrogels before and after swelling

Fourier-transform infrared (FT-IR) measurements were performed using a PerkinElmer Frontier FT-IR combined with a MKII Golden Gate Single Reflection Diamond ATR system from Specac to determine the chemical composition of the hydrogel discs before and after swelling experiments in order to define possible degradation, especially in the cement filtrate. FTIR spectra were recorded for a wavenumber range between 600 and 4000 cm^{-1}. The results were analyzed with PerkinElmer Spectrum Analysis software.

2.8. Mixing procedure of mortar specimens

For preparation of the mortar test specimens, Portland cement (CEM I 52.5 N), standard sand and demineralized water were mixed in a 1:3:0.5 (mass) ratio, following the method described in EN 196-1. Amounts of 450 g cement and 225 g demineralized water were first mixed for 30 s at 140 rpm using a standard mortar mixer. Next, 1350 g sand was added over a period of 30 s while mixing was continued at 140 rpm. The mixing speed was increased to 285 rpm for 30 s. The mixing was stopped for a period of 90 s, while scraping the mortar from the surface of the mixing bowl during the first 30 s of this period. Finally, the mixture was mixed for 60 s at 285 rpm. For the specimens containing SAP (dosed over the cement mass), 0.5 m% (2.25 g) or 1 m% (4.5 g) SAP powder was first dry-mixed with the cement for 60 s before addition of demineralized water. The procedure was then continued as described above. To obtain a similar workability for the mixtures with SAPs as for the reference mixture with a water-to-cement ratio of 0.5, additional water was added in the mixing stage to account for the water taken up by the SAP, which resulted in addition of 10 g g^{-1} extra water for both SAP-containing mixtures [82]. The amount of additional water needed was based on the swelling capacity of the SAP in CF. The workability was measured with a flow test on a jolting table as described in EN 12350-5. The workability was between 181 and 206 mm for all mixtures. The mixtures were molded in beams (40 mm × 40 mm × 160 mm) and cylinders (Ø = 10 mm × 200 mm) as described in EN 196-1 and demolded 24 h after casting. The specimens were wrapped in plastic foil and stored in a climate room with a relative humidity of 95 ± 5% and a temperature of 20 ± 2 °C for 28 days.

2.9. Flexural and compressive strength tests

Flexural strength of the prismatic specimens was measured with a three-point-bending test after 28 days of curing. A compression test was carried out on the resulting parts after the three-point-bending test using a testing machine Walter + Bai DB 250/15. The tests were carried out according to the method described in EN 196-1.

2.10. Air void analysis

A quantitative air void analysis was performed with a RapidAir 457 apparatus. The tests were performed on specimens with dimensions 40 mm × 40 mm × 20 mm, obtained from the mortar beams. The sample surface was polished to create a flat surface and air voids with sharp edges [83]. To enhance the contrast in order to facilitate the analysis, the polished surface was colored with a black marker and white $BaSO_4$ powder was distributed over the surface to fill the voids. The excess of powder was removed with a steel blade and the specimens were mounted in the RapidAir device. All samples were analyzed in two perpendicular directions using three probe lines per frame with a total traverse length of 2413.5 mm and a scanned area of 35 mm × 35 mm, excluding the outer edges. The air void distribution was calculated according to EN 480-11.

2.11. Water permeability tests

The sealing efficiency of the incorporated SAP was studied by water permeability tests. To this end, the mortar cylinders were cut into cylindrical specimens with a diameter of 10 cm and a height of 5 cm at an age of 28 days. The obtained cylindrical specimens were cracked by a controlled Brazilian splitting test. The specimen was put on its side with two metallic sticks attached to it at two opposing positions, the rest of the specimen was fixed with a clamp. Next, the specimen was put between the parallel plates of the pressing machine and they were split in the vertical

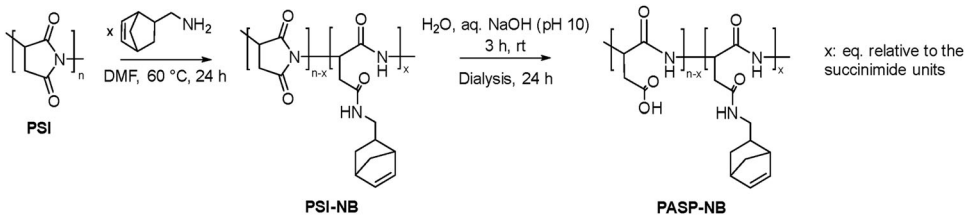

Figure 3. General synthesis scheme of PASP-NB by modification of PSI with NB-NH_2 followed by hydrolysis and dialysis ($x = 0.20$ eq.).

direction (Figure 2a). Silicon pads were used to obtain a nominal crack width of 0.2 mm. The cracked specimens were tied together with steel bands along the circumference to keep the two halves together and to slightly adjust the crack width [85]. The obtained crack widths were studied by microscopy. Pictures of the crack were taken at 5 different positions both at the top and the bottom of the specimens. The measurement spots were marked with a permanent marker to be able to measure the crack width at the same positions after the healing cycles. For each picture, the crack width was measured at 3 positions using the software of the microscope. For each composition, 3 specimens were measured, resulting in a total of 90 measuring points for each composition. This resulted in an average crack width of 0.20 ± 0.02 mm for the reference specimens, 0.22 ± 0.05 mm for the specimens with 0.5 m% SAP and 0.19 ± 0.04 mm for the specimens with 1 m% SAP.

For determination of the water permeability, a constant water-head test was performed [86,87]. A hollow epoxy cylinder was tightly attached to the upper-plane of the cracked specimen with a rubber sealing ring. Sealing grease was applied to seal all openings except for the crack in the specimen (Figure 2b). Demineralized water was added to the cylinder to create a column of water pressing on top of the specimen, resulting in water flowing through the crack. An additional water flow was established at the top of the column to compensate for the water that flows through the specimen in order to keep the level of the water column constant. The whole set-up was put on a tared balance and the change in mass was recorded every minute for a period of 10 min. The water flow rate (g min^{-1}) was calculated by dividing the mass of the water by the time at each recording point. The constant water-head test was carried out on three cylindrical specimens of the same composition for statistical relevance.

After the water permeability tests, the cracked specimens were exposed to wet-dry cycles to induce autogenous healing of the mortar. This was established by immersing the cracked specimens in demineralized water in a reservoir for 12 h. The reservoir was equipped with a pump connected to a timer, which pumped out the water after the period of 12 h, followed by exposure of the specimens to air for 12 h. These cycles were carried out for 28 days. After this period, the crack size and water permeability of the healed specimens were again investigated.

2.12. Microscopic analysis

A microscopic analysis was done to examine the cracks before and after healing and to measure a possible decrease in crack width. A stereomicroscope Leica S8 APO with DFC 295 camera was used. The images were analyzed using Leica software.

2.13. Determination of carbonation depth

The depth of carbonation was analyzed using a phenolphthalein method. After 28 days exposure to wet-dry cycles, the second water permeability test and microscopy analysis, the steel band was removed from the cracked specimens and they were opened along the crack direction to obtain two halves. The cracked surfaces were sprayed with an ethanol solution containing 1% phenolphthalein pH indicator. In the non-carbonated regions on the inner surface of the specimen, the mortar is alkaline and colors purple/pink, while the carbonated regions have a reduced alkalinity and will not show coloration. The depth of the colorless region was measured with a caliper at three points perpendicular to the edge (both at the top and the bottom of the halve) of the split surface. The average depth of carbonation for each specimen was calculated by summing the 6 measuring points per halve specimen for both halves and dividing this value by the total number of measuring points. This method gives a visual indication on the depth of CO_2 penetration and carbonation.

2.14. Statistical analysis

Univariate ANOVA tests with two factors, followed by a Tukey post-hoc test were performed in the statistical program SPSS to identify significant strength differences between the specimens with SAPs and the reference ($p \leq 0.05$).

3. Results and discussion

3.1. Synthesis and characterization of photo-crosslinkable PASP

In order to obtain photo-crosslinkable modified PASP, a PSI precursor was first modified with NB-NH_2 to form PSI-NB as an intermediate, followed by ring-opening of the remaining succinimide rings by alkaline hydrolysis to yield PASP-NB (Figure 3). In a first step, the PSI precursor was synthesized by a condensation polymerization of *L*-aspartic acid with H_3PO_4 according to a modified literature procedure [79]. PSI was obtained as a white solid in 94% yield and a number-average molar mass (M_n) of approximately 16900 g mol^{-1} ($Đ = 2.16$) as determined by GPC measurements. The GPC data can be found in the Supplementary Information (Figure S1). In a second step,

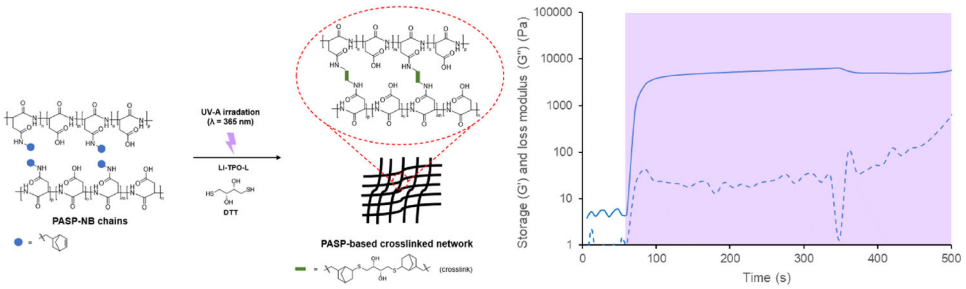

Figure 4. Schematic representation of light-induced crosslinking to form PASP-based networks *via* thiol-ene chemistry (left) and photo-rheological monitoring of the evolution in storage (solid line) and loss modulus (dashed line) of 20 w/v% PASP-NB containing 0.50 eq. DTT and 2 mol% Li-TPO-L upon UV-A induced crosslinking (right).

PSI was reacted with 0.20 eq. (relative to the succinimide units) NB-NH_2, giving PSI-NB *via* nucleophilic attack of the amine on one of the carbonyl moieties in succinimide. The degree of substitution (DS) was approximately 18% as calculated with the relative integrations obtained from ^{1}H-NMR spectra (Figure S2, Supplementary Information). PASP-NB was obtained by alkaline hydrolysis (pH 10) of the PSI-NB to open the remaining succinimide units. The product was dialyzed for 24 h to remove the excess of base and other small molecules that were not removed before by precipitation. PASP-NB was obtained as white/yellow fine powder. The combined yield of the modification of PSI with NB-NH_2 and alkaline hydrolysis was 98%. The ratio of closed succinimide units, opened aspartic acid units and NB-modified aspartic acid units was calculated with the relative integration obtained from ^{1}H-NMR spectra (Figure S3 and Table S1, Supplementary Information).

3.2. Photo-rheology measurements

The potential of PASP-NB to undergo UV-mediated crosslinking in the presence of a bifunctional thiol was studied *via in situ* photo-rheology measurements. The evolution of the storage (G') and loss (G") modulus of a 20 w/v% PASP-NB solution in DDW containing 0.50 eq. DTT and 2 mol% photo-initiator upon UV-irradiation is depicted in Figure 4 (right). Before switching on the UV-light, G' is higher than G", indicating that the solution has more elastic character than liquid character. When the UV-light is switched on, both G' and G" show a steep increase as a result of crosslinking. The steep increase, especially for G', indicates that the crosslinking reaction happens instantly, which is inherent to the selected crosslinking mechanism [88]. Figure 4 (left) shows a schematic representation of the mechanism responsible for network formation. Crosslinking occurs *via* a UV-mediated thiol-ene reaction between -NB on PASP-NB and -SH on DTT initiated by radicals resulting from cleavage of the Li-TPO-L photo-initiator. Since DTT contains two -SH functions, it acts as crosslinker attaching two PASP-NB polymer chains to each other, resulting in a crosslinked network [89]. After the steep increase in G' during the first seconds of UV-irradiation (Figure 4, right), the slope gradually decreases as a result of a decreased reaction rate over time due to diffusion limitations when the network becomes more dense and the reduced concentration of functional groups later in the course of the reaction. Finally, G' reaches a plateau value of approximately 6 kPa shortly after the onset of UV-irradiation, indicating that crosslinking was completed in the first seconds of the UV-irradiation period [90]. No gel point could be identified since there is no cross-over point of G' and G" as the material is already characterized by more pronounced elastic properties prior to crosslinking.

3.3. SAP development and moisture uptake capacity measurements

Hydrogels of PASP-NB were made by gel casting as described in section 2.4, which were afterwards dried by lyophilization, manually grinded with mortar and pestle and sieved to obtain SAP powder. The obtained particles had a nominal particle size $d50 = 134.5 \pm 66.4\,\mu m$ as determined by optical microscopic analysis.

DVS measurements were performed on the grinded SAP powder to determine the equilibrium moisture content as a function of the RH to assess the moisture uptake capacity. After the measurement, two isotherms were obtained that represent the sorption and desorption of moisture by the material (Figure 5). When examining the results, it becomes clear that the material can take up over 100% its own weight at RHs higher than 98%. Furthermore, the material shows a limited hysteresis (difference between the sorption and desorption isotherm) of up to 3.7% at low RHs, indicating that it desorbs most of the initially absorbed moisture again at similar RH. The material can thus serve as a moisture reservoir that absorbs water in a humid environment, retains the water and releases it to hydrate remaining non-hydrated cement particles when no water is able to reach a crack in concrete. Hence, the SAP material is a potential candidate to enhance self-healing properties in concrete.

In Table 2, the moisture uptake capacity of the developed SAP is compared to moisture uptake capacity values of commercially available acrylate-based SAPs A and B found in literature [77]. It is clear that for all selected RHs, the commercial SAPs outperform the developed SAP in terms of moisture uptake capacity. However, the moisture uptake capacity of our material is still high enough to be classified as a SAP [1–3].

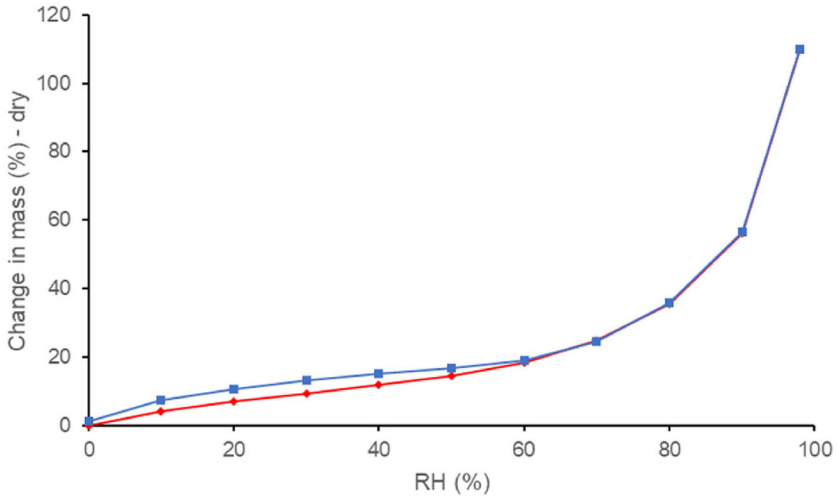

Figure 5. Moisture uptake capacity at varying RH values for PASP-NB SAP represented by a sorption (red curve) and desorption (blue curve) isotherm.

Table 2. Moisture uptake capacity values for PASP-NB SAP compared with two commercially available synthetic acrylate-based SAPs; values for SAP A and B obtained from [77].

Moisture uptake capacity (%)	PASP-NB SAP	SAP A	SAP B
60% RH	19	26	28
90% RH	56	83	84
98% RH	110	394	394

3.4. Swelling experiments

Structure elucidation of the hydrogel discs was done by FT-IR spectroscopy before the swelling experiments. The FT-IR spectrum can be found in the Supplementary Information (Figure S4) and assignment of the most important peaks was done based on FT-IR spectra of unmodified PASP found in literature [91].

The equilibrium swelling ratio of the developed SAP was determined both in DDW and CF solution to gain insight in the swelling capacity of the material. Also the gel fraction was determined by means of equilibrium swelling in DDW for 3 days. A moderate gel fraction of 67.4 ± 1.4% was found, which indicates a limited efficiency of the crosslinking reaction and the presence of a large fraction of non-crosslinked species in the network. This moderate gel fraction implies that 67% of the material is crosslinked SAP, while the other 33% is non-crosslinked PASP-NB and DTT, which dissolved and leached out during the swelling experiment. This could be a reason for the non-linear behavior observed, for example in the mortar strength, as will be discussed in the next paragraphs. The recorded equilibrium swelling ratio of the hydrogel discs after 3 days in DDW was 128.8 ± 8.7 g g^{-1}, meeting the requirement for being a superabsorbent material (swelling capacities of 10 to 1000 g g^{-1}) [23]. The sorption capacity of the SAP powder was obtained *via* the filtration method, resulting in a value of 115.4 ± 9.9 g g^{-1}, which is slightly lower than the value found for the hydrogel discs. This is possibly a consequence of the different measuring techniques for the sorption capacity of the hydrogel discs on the one hand and the SAP powder on the other hand, causing small variations in the result. Nevertheless, for further discussion and comparison to the commercial SAPs, only the sorption capacity value for the powder will be considered. The obtained sorption capacity is, however, significantly lower compared to that of commercial SAPs A and B (305.0 ± 3.7 g g^{-1} and 283.2 ± 2.4 g g^{-1} respectively) [54].

A drastic decrease of the sorption capacity to 3.8 ± 0.3 g g^{-1} was observed for the hydrogel discs after 3 days incubation in the CF solution, which corresponds to a reduction of 97% compared to the sorption capacity in water. For the powder, a slightly higher sorption capacity of 14.3 ± 3.9 g g^{-1} was observed when using the filtration method, which is a reduction of 87.6%. A decreased sorption capacity in CF solution is also reported for the commercial SAPs, *i.e.* 61.0 ± 1.0 g g^{-1} for SAP A and 58.4 ± 1.7 g g^{-1} for SAP B [54]. The sorption capacities for the commercial SAPs were also obtained after 24 h incubation followed by filtration as recommended by RILEM TC 260-RSC testing strategy for determining the sorption of SAPs [81]. The strongly reduced sorption capacity can be attributed to two main factors. First, CF solution is a highly alkaline solution with pH 12.6, which implies that the aspartic acid units of the polymer network structure will be deprotonated, resulting in the formation of anionic carboxylate moieties. Normally, this would result in a higher sorption capacity due to the repelling effect of the negative charges, but this effect is counterbalanced by the charge-screening effect of the cations present in the CF, which reduces the osmotic pressure that is responsible for absorption [77,92,93]. Second, the multivalent cations present, especially Ca^{2+} and Mg^{2+}, can form physical crosslinks with the carboxylate anions by complexation, resulting in a denser network and hence a reduced swelling capacity [72,94,95]. The reduced sorption capacity of the SAPs in CF is however beneficial in the preparation stage of the mortar specimens as a high swelling ability results in the need for addition of high amounts of additional water to account for the uptake of the mixing water to obtain a good workability and the

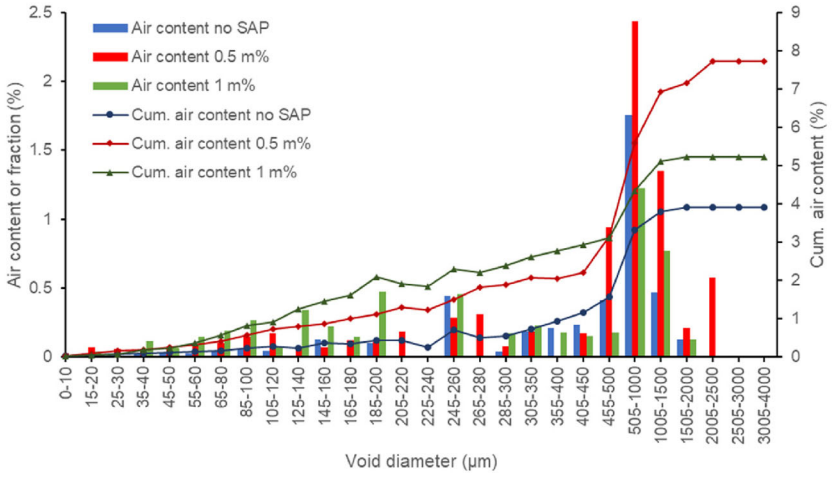

Figure 6. Void size distribution and cumulative air content of the reference specimen (blue), specimen with 0.5 m% SAP (red) and specimen with 1 m% SAP (green); the bars show the size distribution of the air voids and the curves show the cumulative air content for the whole specimen.

creation of larger macropores, which will negatively influence the strength of the mortar specimens [82].

3.5. Air void analysis

An air void analysis was performed on all specimens to determine the total amount of voids and macropores and to assess the influence of SAPs on the total air content, considering incorporation of SAPs generally results in a higher air content [45,82,96]. This was confirmed by an increased cumulative air content to 7.7% for 0.5 m% and 5.2% for 1 m% SAP compared to the reference (cumulative air content of 3.9%) (Figure 6). The results are not as expected since the air content usually follows the same trend as the amount of SAP added to the specimen. This could be linked to the moderate gel fraction of the SAPs, as described in section 3.4. The presence of non-cross-linked materials (*i.e.* the sol fraction), is likely to cause this non-linear behavior. Another reason could be the relatively low swelling capacity of the SAP in CF, nullifying the effect of the SAP content on the macro pore formation [82]. The porosity of the specimens was calculated after image analysis of the specimens (Figure 7.) as the percentage of pores (share of the white spaces on the total surface) for the specimens with SAPs minus the percentage of pores found for the reference. This resulted in a calculated porosity of 3.4% for 0.5 m% SAP and 2.3% for 1 m% SAP. When visually inspecting the images of the treated surfaces, it also becomes clear that more pores are visible on the surfaces with SAPs compared to the reference. These are mostly macropores as more water is added to the mixture when SAPs are present, resulting in a higher amount of large air voids. Addition of SAPs, independent of the amount, results in a reduced strength as the voids created by the SAP form a pathway for crack progression and reduce the cross-sectional area [97]. Furthermore, when comparing the void size distribution in Figure 6, it is clear that the specimen with 0.5 m% SAP shows a higher fraction of large macropores (diameter 455–2500 µm) than the specimen with 1 m% SAP, which further supports later observations since the strength is highly influenced by the content of macropores. The SAPs in the saturated form were characterized by sizes between 100 and 450 µm.

3.6. Evaluation of the mechanical strength of mortar samples

The results of the three-point bending and compression tests to determine the flexural/bending strength and the compressive strength upon addition of 0.5 m% and 1 m% PASP-NB SAP are summarized in Figure 8. An univariate ANOVA test followed by a Tukey post-hoc test showed that the flexural strength reductions upon addition of SAP compared to the reference specimen are significant ($p < 0.05$), both upon addition of 0.5 m% and 1 m% SAP. A non-linear trend in tensile strength reduction with increasing fraction of SAP can be observed. A reduction of 24% was found for 0.5 m% while addition of 1 m% only resulted in a reduction of 12%, which is opposite to what has usually been described in literature [45,82,98,99]. This is a result of the lower air content and formation of smaller macropores in case of 1 m% SAP compared to 0.5 m% SAP, as the bending strength decreases with increasing amount of air voids and macropores in the cross-sectional area of the imposed tensile plane [100]. This observation was indeed confirmed by the air void analysis described in section 3.5.

However, the compressive strength results also provide insight in the influence of the macropore formation. Statistical analysis of the results for the compressive strength showed a significant difference between the reference specimen and both SAP-containing specimens. The strength reductions were 24% and 28% compared to the reference for 0.5 m% and 1 m%, respectively. There was no significant reduction observed between the two SAP-containing specimens. The decrease in compressive strength can be attributed to an irregular shape of the SAP particles and higher amount of macroporosity with increasing SAP content. This results in formation of irregular macropores and consequently, the compressive load is not transferred equally by dome actions, as would

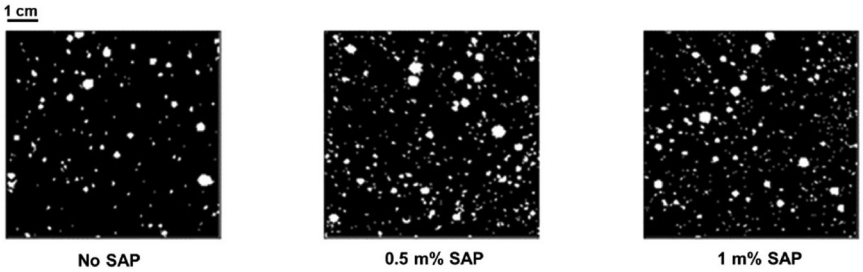

Figure 7. Observed air voids on the treated surfaces by air void analysis.

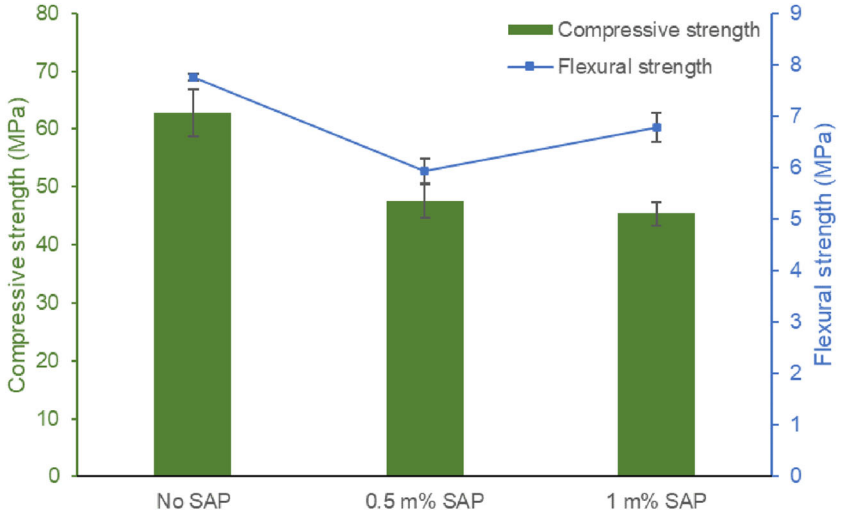

Figure 8. Effect of the addition of 0.5 m% and 1 m% PASP-NB SAP on the flexural and compressive strength of mortar specimens.

be the case for spherical SAPs, resulting in a lower compressive strength compared to the reference specimen [100]. The flexural strength is less influenced by the irregular shape of the pores as it is mainly determined by the total amount of macropores in the cross-sectional area of the tensile plane.

When comparing the results for the bending strength to the values obtained when adding equal amounts of commercial SAP, our developed SAP is inferior to SAP B (4% strength gain and 0% strength reduction for 0.5 m% and 1 m% respectively) and to 0.5 m% SAP A (1% strength gain). When adding 1 m% SAP A, a similar tensile strength reduction of 14% is observed as for our SAP. When considering the compressive strength, our SAP outperforms SAP A (36% and 56% reduction for 0.5 m% and 1 m% respectively), while SAP B shows results (22% reduction both for 0.5 m% and 1 m%) which are in line with our SAP. SAP A, has a nominal particle size of 100.0 ± 21.5 µm and an absorption capacity of 61.0 ± 1.0 g g^{-1} in CF, while our SAP has a particle size of 134.5 ± 66.4 µm and an absorption capacity of 14.3 ± 3.9 g g^{-1} in CF. SAP B, has a particle size of 476.6 ± 52.9 µm and an absorption capacity of 58.0 ± 2.0 g g^{-1}. The composition of the mortar specimens was the same as the mixture used in our research and a workability between 200 and 220 mm was found for all compositions. This corresponded to addition of 30.5 g g^{-1} extra water for SAP A and 8.9 g g^{-1} extra water for SAP B. The higher amount of added water in case of SAP A results in a larger macroporosity and a larger strength reduction compared to SAP B (values for SAP A and B retrieved from [77,100]).

3.7. *Self-sealing and self-healing properties of the developed SAP*

Water permeability measurements were carried out to assess the sealing potential of the SAP in the mortar specimens. The average water flow after 10 min of recording for three cracked cylindrical specimens per composition and the accompanying reduction as result of SAP incorporation are summarized in Table 3.

Significant differences ($p < 0.05$) are observed in water flow between the reference and the specimens containing 0.5 m% and 1 m% SAP. Incorporation of SAPs results in a reduction by half of the original water flow. There is no significant difference between the two SAP-containing specimens (50% reduction in water flow for 0.5 m% compared to 54% for 1 m%). This confirms the strong sealing potential of the SAP and a partially regained watertightness of the concerned specimen [61,77]. Self-sealing in concrete by incorporation of SAPs is mainly attributed to the high intrinsic swelling capacity of the SAP. As discussed before, SAPs create pores in the specimen due to swelling in the mixing stage and settle down in these pores when deswelling during the curing stage. When a crack forms in the specimen and external fluid can infiltrate into the crack, the SAPs present in the pores at the edges of the crack take up the water and swell,

Table 3. Reduction in water permeability as a result of sealing due to presence of SAPs in the specimen before and after 28 days of wet-dry cycles, obtained water flow was recorded after 10 min measuring time.

	Water flow ($g\ min^{-1}$) - before	Reduction (%)	Water flow ($g\ min^{-1}$) - after	Reduction compared to before healing cycles (%)
No SAP	26.3 ± 3.4	–	10.0 ± 2.4	62 ± 9
0.5 m% SAP	13.3 ± 3.0	50 ± 11	5.6 ± 1.2	58 ± 9
1 m% SAP	12.4 ± 0.3	54 ± 6	5.3 ± 4.7	56 ± 39

filling up the crack. This results in blockage of the crack and a partial or in some cases even completely regained watertightness [16,49,65]. Generally, a higher fraction of SAP results in a more pronounced self-sealing. Considering the results in Table 3, it is clear that the effect of a higher SAP content is minimal in this case. When considering Figure 9, it becomes clear that the sealing effect by the SAPs happens instantly after first contact with water, since the total mass of water passing through the specimens with SAP is already decreased during the first minutes of the measuring period compared to the reference specimens.

The self-healing potential of the SAP was investigated by subjecting the specimens to a second water permeability test after 28 days exposure to wet-dry healing cycles. Also the crack size was studied again *via* microscopy to identify crack closure and the possible formation of healing products. The average crack size for the reference specimen was reduced to 0.18 ± 0.03 mm, compared to 0.20 ± 0.02 mm before the healing cycles. For the specimens with SAPs, an average crack size of 0.18 ± 0.03 mm was observed for 0.5 m% after healing compared to 0.22 ± 0.05 mm before, and 0.15 ± 0.02 mm was observed after healing for 1 m% compared to 0.19 ± 0.04 mm before. When comparing the average water flow before and after the healing cycles in Table 3, it is clear that the water flow is significantly reduced for all specimens. The reference shows the largest reduction (62%) after the healing cycles as a result of autogenous healing of the mortar. In the specimens with SAPs, autogenous healing results in an additional reduction of water flow with 58% and 56% for 0.5 m% and 1 m% SAP respectively, on top of the reduction due to self-sealing. Hence, the combination of self-sealing and autogenous healing reduces the water permeability with 79% for 0.5 m% SAP and 80% for 1 m% SAP compared to the reference specimens containing no SAPs before the healing cycles. Even after curing, non-hydrated cement particles are usually present in the mortar matrix, especially for young mortar. Water that is infiltrating in the crack can hydrate these particles with formation of new calcium silicate hydrates that can seal small cracks [62,101]. Another mechanism for autogenous healing, which is more dominant especially for mortar at a later age, is the formation of $CaCO_3$ by reaction of the $Ca(OH)_2$ present with CO_2 from the air and dissolved in water entering the crack. The $CaCO_3$ precipitates out of the matrix as a white crystalline substance that can block the crack [61,102]. Generally, these combined mechanisms result in complete healing of small cracks (30 − 50 μm) and partial healing of larger cracks (up to 150 μm) [50,54,63,64]. When examining microscopy images of the crack before and after the wet-dry cycles, the formation of healing products was observed as white crystalline precipitates on the crack surface, both for the reference specimens as for the specimens with SAPs (Figure 10).

Wet-dry cycles are an excellent method to promote autogenous healing [63], but incorporation of SAPs can be a tool to further enhance healing. SAPs take up large amounts of water during a wet cycle, which can be slowly released during a dry cycle. In this way, there is a continuous water supply to promote the healing [54]. If at least 1 h of contact with water is achieved each day, SAPs can stimulate further hydration up to 40% compared to materials without added SAPs [101]. However, in this research, there is no significant difference observed in water permeability between the three specimen compositions after the healing cycles. The main reason for the regained watertightness after wet-dry cycles is the autogenous healing of the mortar itself, next to the swelling action of the SAP. As depicted in Figure 10, healing occurred for all specimens independent of the presence of SAPs, but it is not possible to quantitatively determine the extent to which healing occurred for each specimen composition, as only the surface of the cracked specimens was investigated. As the initial swelling by the SAPs led to an initial lower water flow, no conclusion can be drawn on the improvements of healing as such as a subsequent permanent sealing due to healing is masked.

The carbonation depth was visualized by phenolphthalein treatment of the broken specimens (Figure 11). When examining the picture, it becomes clear that an increasing SAP content results in a reduced carbonation depth (7.4 ± 1.2 mm for 0.5 m% and 7.8 ± 1.7 mm for 1 m%) compared to the reference specimen (10.0 ± 1.5 mm). The pH of the non-carbonated region is in the range of 11.5 to 12.5 due to the high content of alkaline $Ca(OH)_2$, resulting in the phenolphthalein indicator turning purple/pink. Carbonation of $Ca(OH)_2$ with CO_2, with formation of neutral $CaCO_3$, creates neutral regions that remain colorless when treated with phenolphthalein. In this way, the border between carbonated and non-carbonated mortar can be visualized [103]. However, with the phenolphthalein method it is not possible to quantitatively determine the carbonation depth. The region of color change for this pH indicator is between pH 8.0 and 9.8, hence partially carbonated zones where both $Ca(OH)_2$ and $CaCO_3$ are present, show a less pronounced color change and are difficult to identify [104,105]. Also, this method cannot give quantitative information on the formed healing products inside the specimens as the formed crystals might be damaged or lost when breaking the specimens for the analysis. Quantification of healing products requires other non-

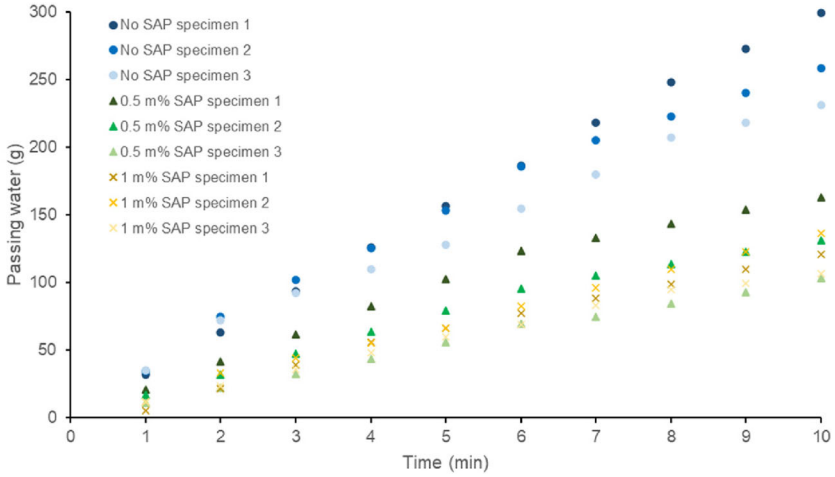

Figure 9. Water passing through the crack as a function of time for all specimen compositions recorded for a period of 10 min.

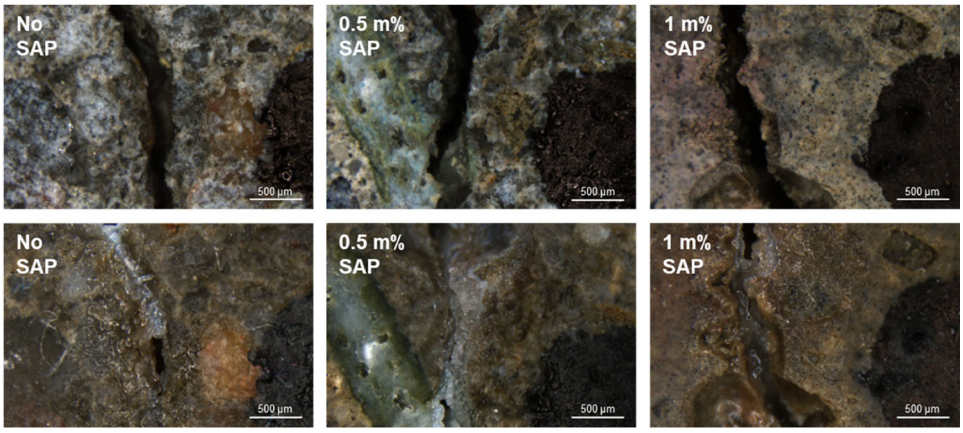

Figure 10. Microscopy images of the cracked specimens before (top images) and after healing cycles (bottom images) that show the formation of $CaCO_3$ as white crystalline deposit inside the crack.

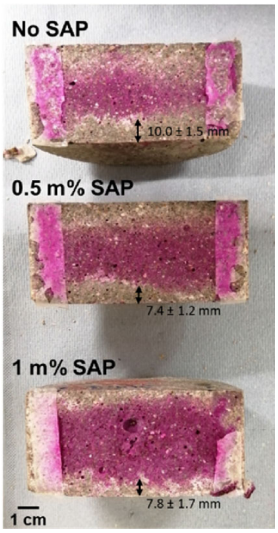

Figure 11. Cross-section of the split specimens after wet-dry cycles and treatment with phenolphthalein solution to indicate the depth of carbonation of the reference specimen (top), the specimen with 0.5 m% SAP (middle) and with 1 m% SAP (bottom).

destructive methods, *e.g.* X-ray computed microtomography [55]. Nevertheless, this method is a useful tool to get a first visual indication on the depth of CO_2 penetration and subsequent carbonation. In this case, it does show that CO_2 penetrated deeper in the core of the crack for the reference, while carbonation is only limited to the areas in contact with air at the surface of the specimens in the presence of SAPs, indicating that SAPs to some extent shield the core of the crack from the outer environment during the wet-dry cycles. The SAPs present in the crack of the specimens swell due to the high water uptake capacity and the SAPs close to the surface can shield the core of the crack, making it harder for water and gaseous CO_2 to enter the interior of the crack and go through the material plane. As a result of the limited penetration depth of CO_2, the carbonation depth will also be reduced. The sealing effect of the SAPs also partially seals the cementitious matrix from intruding CO_2. This apparent wetter surface was also visually noticed. Furthermore, the carbonation rate will be the highest at moderate internal RH (between 40 and 80%) since a low RH results in insufficient water being present in the pores to dissolve the CO_2 to allow a reaction with $Ca(OH)_2$ and at high RH, the pores will be saturated, slowing down the diffusion of CO_2 [106]. In that way, the effect of the SAPs on the carbonation of the concrete is dual, as they will also reduce the RH inside concrete by absorption of the water present and blocking further ingression of water, causing the carbonation rate to decrease.

4. Conclusions

The present work reports the synthesis of norbornene-modified poly(aspartic acid) and subsequent crosslinking in the presence of a thiol crosslinker to obtain a biobased SAP. DVS and swelling experiments in DDW showed that the obtained material had a water absorption capacity of more than 100 times its own weight while showing limited hysteresis, indicating its potential to be used as a SAP, in this work as additive for mortar matrices. The sorption capacity in CF drastically decreased due to the presence of divalent cations, which is in line with previously reported values for commercial acrylate-based SAPs, and FT-IR spectra showed that no degradation occurred as a result of the highly alkaline conditions. Flexural strength tests showed a reduction in strength which displayed a non-linear trend with increasing SAP content (24% for 0.5 m% SAP compared to 12% for 1 m% SAP). This was supported by a higher air content and a higher fraction of macropores with large void diameters for 0.5 m% compared to 1 m% SAP. A similar reduction in compressive strength was observed for both tested SAP contents. Furthermore, the SAPs efficiently reduced the water permeability with more than 50% after 10 min of water flow for cracked mortar specimens with a crack width of 0.19 to 0.22 mm, with sealing of the crack from the first contact with water. Healing of the mortar specimens was observed after water permeability tests and microscopy analysis after wet-dry cycles, independent of the presence of SAPs. For the reference specimens, water permeability decreased with 62% compared to the water permeability before exposure to wet-dry cycles, indicating autogenous healing of the mortar. For the specimens containing SAPs, an additional reduction in water permeability of 58% for 0.5 m% SAP and 56% for 1 m% SAP was observed on top of the reduction that was already observed before exposure to the wet-dry cycles due to the sealing effect of the SAPs. Visualization of the carbonation depth with phenolphthalein showed that swelling of SAPs can efficiently shield the interior of the crack and partially blocks gaseous CO_2 from entering the crack, resulting in a reduced carbonation depth. In summary, the developed SAP is an excellent candidate to enhance self-sealing in mortar. The effect of the SAPs on the healing of mortar is on the other hand limited. Incorporation of the developed SAPs results in strength reduction of the mortar. The tensile strength reduction due to our SAP (24% for 0.5 m% SAP compared to 12% for 1 m% SAP) is larger compared to commercial SAPs (1% strength gain and 14% strength reduction for 0.5 m% and 1 m% SAP A respectively, 4% strength gain and 0% strength reduction for 0.5 m% and 1 m% SAP B respectively), but our SAP (24% and 28% reduction for 0.5 m% and 1 m% respectively) outperforms SAP A in terms of compressive strength (36% and 56% reduction for 0.5 m% and 1 m% respectively) while it shows similar results as for SAP B (22% reduction both for 0.5 m% and 1 m%). However, since the SAP can be considered as a moisture reservoir able to efficiently release the absorbed water at low RHs (proven by the limited hysteresis observed in DVS), more in-depth analyses are necessary to draw a conclusion on the effect of the SAPs on the healing of the mortar. However, since the developed SAP is biobased and has good self-sealing properties, it could be a valuable alternative for fossil-based acrylic commercial SAPs to reduce the negative impact on the environment. The present work could therefore be a starting point to further study this class of biobased SAPs in applications considering sustainable concrete repair, which mainly involves development of green SAPs and SAP recycling [107].

Acknowledgements

This research was carried out in the framework of project 'GREENER'. Project 'GREENER' is financed by the Interreg V program Flanders-The Netherlands, the cross-border collaboration with financial support of the European Fund for Regional Development with co-financing from province East Flanders and the Ministry of Economical Affaires and Climate (The Netherlands). More information: www.grensregio.eu.

Disclosure statement

No potential conflict of interest was reported by the author(s).

Funding

This work was supported by Interreg Vlaanderen-Nederland and province Oost-Vlaanderen (Belgium).

ORCID

Lauren De Grave http://orcid.org/0000-0003-1472-6278
José Roberto Tenório Filho http://orcid.org/0000-0002-3135-5694
Didier Snoeck http://orcid.org/0000-0001-9427-6312
Nele De Belie http://orcid.org/0000-0002-0851-6242
Katrien V. Bernaerts http://orcid.org/0000-0002-2939-2963
Sandra Van Vlierberghe http://orcid.org/0000-0001-7688-1682

References

[1] Zohuriaan-Mehr MJ, Omidian H, Doroudiani S, et al. Advances in non-hygienic applications of superabsorbent hydrogel materials. J Mater Sci. 2010;45(21):5711–5735.
[2] Mechtcherine V, Wyrzykowski M, Schröfl C, et al. Application of super absorbent polymers (SAP) in concrete construction—update of RILEM state-of-the-art report. Mater Struct. 2021;54(2):80.
[3] Schröfl C, Erk KA, Siriwatwechakul W, et al. Recent progress in superabsorbent polymers for concrete. Cem Concr Res. 2022;151:106648.
[4] Zohuriaan-Mehr MJ, Kabiri K. Superabsorbent polymer materials: a review. Iran Polym J. 2008;17:447–451.
[5] Caló E, Khutoryanskiy VV. Biomedical applications of hydrogels: a review of patents and commercial products. Eur Polym J. 2015;65:252–267.

[6] Dey S, Kenneally D, Odio M, et al. Modern diaper performance: construction, materials, and safety review. Int J Dermatol. 2016;55:18–20.
[7] Sadeghi M, Hosseinzadeh H. Synthesis of starch—poly(sodium acrylate-co-acrylamide) superabsorbent hydrogel with salt and pH-responsiveness properties as a drug delivery system. J Bioact Compat Polym. 2008; 23(4):381–404.
[8] Kim DW, Kim KS, Seo YG, et al. Novel sodium fusidate-loaded film-forming hydrogel with easy application and excellent wound healing. Int J Pharm. 2015; 495(1):67–74.
[9] Davies LC, Novais JM, Martins-Dias S. Detoxification of olive mill wastewater using superabsorbent polymers. Environ Technol. 2004;25(1):89–100.
[10] Hüttermann A, Orikiriza LJB, Agaba H. Application of superabsorbent polymers for improving the ecological chemistry of degraded or polluted lands. Clean Soil Air Water. 2009;37(7):517–526.
[11] Demitri C, Scalera F, Madaghiele M, et al. Potential of cellulose-based superabsorbent hydrogels as water reservoir in agriculture. Int J Polym Sci. 2013;2013: 1–6.
[12] Parvathy PC, Jyothi AN, John KS, et al. Cassava starch based superabsorbent polymer as soil conditioner: Impact on soil physico-chemical and biological properties and plant growth. Clean Soil Air Water. 2014;42(11):1610–1617.
[13] Guilherme MR, Aouada FA, Fajardo AR, et al. Superabsorbent hydrogels based on polysaccharides for application in agriculture as soil conditioner and nutrient carrier: a review. Eur Polym J. 2015;72: 365–385.
[14] Thombare N, Mishra S, Siddiqui MZ, et al. Design and development of guar gum based novel, superabsorbent and moisture retaining hydrogels for agricultural applications. Carbohydr Polym. 2018;185:169–178.
[15] Ostrand MS, DeSutter TM, Daigh ALM, et al. Superabsorbent polymer characteristics, properties, and applications. Agrosystems, Geosci Environ. 2020;3: e20074.
[16] Mignon A, Snoeck D, Dubruel P, et al. Crack mitigation in concrete: Superabsorbent polymers as key to success? Materials (Basel). 2017;10(3):237.
[17] Torres-Lugo M, Peppas NA. Molecular design and in vitro studies of novel pH-sensitive hydrogels for the oral delivery of calcitonin. Macromolecules. 1999; 32(20):6646–6651.
[18] Pourjavadi A, Barzegar S. Synthesis and evaluation of pH and thermosensitive pectin-based superabsorbent hydrogel for oral drug delivery systems. Starch - Stärke. 2009;61(3–4):161–172.
[19] Mignon A, De Belie N, Dubruel P, et al. Superabsorbent polymers: a review on the characteristics and applications of synthetic, polysaccharide-based, semi-synthetic and 'smart' derivatives. Eur Polym J. 2019;117:165–178.
[20] Zohuriaan-Mehr MJ, Pourjavadi A, Salimi H, et al. Protein- and homo poly(amino acid)-based hydrogels with super-swelling properties. Polym Adv Technol. 2009;20(8):655–671.
[21] Narune A, Prasad E, Allied Market Research [Internet]. Super absorbent polymer market by type (synthetic and natural), application (personal care, healthcare, agriculture & horticulture, and others), and production method (suspension polymerization, solution polymerization, and gel polymerization). [cited 2022 Mar 11]. Available from: https://www.alliedmarketresearch.com/super-absorbent-polymers-market.
[22] Thombre SM, Sarwade BD. Synthesis and biodegradability of polyaspartic acid: a critical review. J Macromol Sci Part A Pure Appl Chem. 2005;42(9): 1299–1315.
[23] Sharma S, Dua A, Malik A. Polyaspartic acid based superabsorbent polymers. Eur Polym J. 2014;59: 363–376.
[24] Nakato T, Yoshitake M, Matsubara K, et al. Relationships between structure and properties of poly(aspartic acid)s. Macromolecules. 1998;31(7): 2107–2113.
[25] Adelnia H, Tran HDN, Little PJ, et al. Poly(aspartic acid) in biomedical applications: from polymerization, modification, properties, degradation, and biocompatibility to applications. ACS Biomater Sci Eng. 2021; 7(6):2083–2105.
[26] Jalalvandi E, Shavandi A. Polysuccinimide and its derivatives: Degradable and water soluble polymers (review). Eur Polym J. 2018;109:43–54.
[27] Adelnia H, Blakey I, Little PJ, et al. Hydrogels based on poly(aspartic acid). Synthesis Appl. Front Chem. 2019;7:755.
[28] Salakhieva DV, Gumerova DR, Akhmadishina RA, et al. Anti-Radical and cytotoxic activity of polysuccinimide and polyaspartic acid of different molecular weight. BioNanoSci. 2016;6(4):348–351.
[29] Zakharchenko S, Sperling E, Ionov L. Fully biodegradable self-rolled polymer tubes: a candidate for tissue engineering scaffolds. Biomacromolecules. 2011;12(6):2211–2215.
[30] Juriga D, Nagy K, Jedlovszky-Hajdú A, et al. Biodegradation and osteosarcoma cell cultivation on poly(aspartic acid) based hydrogels. ACS Appl Mater Interfaces. 2016;8(36):23463–23476.
[31] Stroganov V, Pant J, Stoychev G, et al. 4D biofabrication: 3D cell patterning using shape-changing films. Adv Funct Mater. 2018;28(11):1706248.
[32] Xu M, Zhao Y, Feng M. Polyaspartamide derivative nanoparticles with tunable surface charge achieve highly efficient cellular uptake and low cytotoxicity. Langmuir. 2012;28(31):11310–11318.
[33] Dou XB, Hu Y, Zhao NN, et al. Different types of degradable vectors from low-molecular-weight polycation-functionalized poly(aspartic acid) for efficient gene delivery. Biomaterials. 2014;35(9):3015–3026.
[34] Ma C, Zhang J, Guo L, et al. Cyclen grafted with poly[(aspartic acid)- co -Lysine]: preparation, assembly with plasmid DNA, and in vitro transfection studies. Mol Pharm. 2016;13(1):47–54.
[35] Salakhieva D, Shevchenko V, Németh C, et al. Structure–biocompatibility and transfection activity relationships of cationic polyaspartamides with (dialkylamino)alkyl and alkyl or hydroxyalkyl side groups. Int J Pharm. 2017;517(1-2):234–246.
[36] Yavvari PS, Verma P, Mustfa SA, et al. A nanogel based oral gene delivery system targeting SUMOylation machinery to combat gut inflammation. Nanoscale. 2019;11(11):4970–4986.
[37] Han S, Liu Y, Nie X, et al. Efficient delivery of antitumor drug to the nuclei of tumor cells by amphiphilic biodegradable poly(L-Aspartic acid-co-Lactic acid)/ DPPE co-polymer nanoparticles. Small. 2012;8(10): 1596–1606.
[38] Park CW, Yang H-M, Woo M-A, et al. Completely disintegrable redox-responsive poly(amino acid) nanogels for intracellular drug delivery. J Ind Eng Chem. 2017;45:182–188.
[39] Budai-Szűcs M, Kiss E, Szilágyi B, et al. Mucoadhesive cyclodextrin-modified thiolated poly(aspartic acid) as a potential ophthalmic drug delivery system. Polymers (Basel). 2018;10(2):199.
[40] Krisch E, Gyarmati B, Barczikai D, et al. Poly(aspartic acid) hydrogels showing reversible

volume change upon redox stimulus. Eur Polym J. 2018;105:459–468.
[41] Sim T, Lim C, Cho YH, et al. Development of pH-sensitive nanogels for cancer treatment using cross-linked poly(aspartic acid- graft -imidazole)- block -poly(ethylene glycol). J Appl Polym Sci. 2018; 135(20):46268.
[42] Yang J, Wang F, Fang L, et al. The effects of aging tests on a novel chemical sand-fixing agent – polyaspartic acid. Compos Sci Technol. 2007;67(10): 2160–2164.
[43] Wei J, Yang H, Cao H, et al. Using polyaspartic acid hydro-gel as water retaining agent and its effect on plants under drought stress. Saudi J Biol Sci. 2016; 23(5):654–659.
[44] Lü S, Feng C, Gao C, et al. Multifunctional environmental smart fertilizer based on l-Aspartic acid for sustained nutrient release. J Agric Food Chem. 2016; 64(24):4965–4974.
[45] Jensen OM, Hansen PF. Water-entrained cement-based materials: I. Principles and theoretical background. Cem Concr Res. 2001;31(4):647–654.
[46] Craeye B, Geirnaert M, De Schutter G. Super absorbing polymers as an internal curing agent for mitigation of early-age cracking of high-performance concrete bridge decks. Constr Build Mater. 2011;25(1):1–13.
[47] Mechtcherine V, Gorges M, Schroefl C, et al. Effect of internal curing by using superabsorbent polymers (SAP) on autogenous shrinkage and other properties of a high-performance fine-grained concrete: results of a RILEM round-robin test. Mater Struct. 2014;47(3): 541–562.
[48] Justs J, Wyrzykowski M, Bajare D, et al. Internal curing by superabsorbent polymers in ultra-high performance concrete. Cem Concr Res. 2015;76:82–90.
[49] Lee HXD, Wong HS, Buenfeld NR. Potential of superabsorbent polymer for self-sealing cracks in concrete. Adv Appl Ceram. 2010;109(5):296–302.
[50] Snoeck D, Steuperaert S, Van Tittelboom K, et al. Visualization of water penetration in cementitious materials with superabsorbent polymers by means of neutron radiography. Cem Concr Res. 2012;42(8): 1113–1121.
[51] Hong G, Choi S. Rapid self-sealing of cracks in cementitious materials incorporating superabsorbent polymers. Constr Build Mater. 2017;143:366–375.
[52] Tenório Filho JR, Vermoesen E, Mannekens E, et al. Enhanced durability performance of cracked and uncracked concrete by means of smart in-house developed superabsorbent polymers with alkali-stable and -unstable crosslinkers. Constr Build Mater. 2021;297: 123812.
[53] Lee HXD, Wong HS, Buenfeld NR. Self-sealing of cracks in concrete using superabsorbent polymers. Cem Concr Res. 2016;79:194–208.
[54] Snoeck D, Van Tittelboom K, Steuperaert S, et al. Self-healing cementitious materials by the combination of microfibres and superabsorbent polymers. J Intell Mater Syst Struct. 2014;25(1):13–24.
[55] Snoeck D, Dewanckele J, Cnudde V, et al. X-ray computed microtomography to study autogenous healing of cementitious materials promoted by superabsorbent polymers. Cem Concr Compos. 2016;65:83–93.
[56] Araújo M, Van Vlierberghe S, Feiteira J, et al. Cross-linkable polyethers as healing/sealing agents for self-healing of cementitious materials. Mater Des. 2016;98: 215–222.
[57] Van Tittelboom K, De Belie N, De Muynck W, et al. Use of bacteria to repair cracks in concrete. Cem Concr Res. 2010;40(1):157–166.
[58] Pareek S, Shrestha KC, Suzuki Y, et al. Feasibility of externally activated self-repairing concrete with epoxy injection network and Cu-Al-Mn superelastic alloy reinforcing bars. Smart Mater Struct. 2014;23(10): 105027.
[59] Ryu J-S. An experimental study on the repair of concrete crack by electrochemical technique. Mat Struct. 2001;34(7):433–437.
[60] Hager MD, Greil P, Leyens C, et al. Self-healing materials. Adv Mater. 2010;22(47):5424–5430.
[61] Edvardsen C. Water permeability and autogenous healing of cracks in concrete. ACI Mater J. 1999;96: 448–454.
[62] Wu M, Johannesson B, Geiker M. A review: Self-healing in cementitious materials and engineered cementitious composite as a self-healing material. Constr Build Mater. 2012;28(1):571–583.
[63] Yang Y, Lepech MD, Yang E-H, et al. Autogenous healing of engineered cementitious composites under wet–dry cycles. Cem Concr Res. 2009;39(5):382–390.
[64] Snoeck D, De Belie N. From straw in bricks to modern use of microfibers in cementitious composites for improved autogenous healing – A review. Constr Build Mater. 2015;95:774–787.
[65] Van Tittelboom K, Wang J, Araújo M, et al. Comparison of different approaches for self-healing concrete in a large-scale lab test. Constr Build Mater. 2016;107:125–137.
[66] Tsuji M, Okuyama A, Enoki K, et al. Development of new concrete admixture 618. preventing from leakage of water through cracks. JCA Proc Cem Concr. 1998; 52:418–423.
[67] Jensen OM, Hansen PF. Water-entrained cement-based materials: II. Experimental observations. Cem Concr Res. 2002;32(6):973–978.
[68] Tangkokiat P, Thanapornpavornkul T, Muangkaew S, et al. Characterization of neutral versus anionic superabsorbent polymers (SAPs) in ion-rich solutions for their use as internal curing agents. 3rd Int Conf Appl Superabsorbent Polym Other New Admixtures Towar Smart Concr. 2020. p. 38–45.
[69] Tenório Filho JR, Mannekens E, Van Tittelboom K, et al. Innovative SuperAbsorbent polymers (iSAPs) to construct crack-free reinforced concrete walls: An in-field large-scale testing campaign. J Build Eng. 2021; 43:102639.
[70] Zlopasa J, Koenders E, Picken S. A novel bio-based curing compound for cement-based materials. In: Mechtcherine V, Schröfl C, editors. Int RILEM conf appl superabsorbent polym other new admixtures concr constr. France: RILEM publications S.A.R.L.; 2014. p. 47.
[71] Wang J, Mignon A, Snoeck D, et al. Application of modified-alginate encapsulated carbonate producing bacteria in concrete: a promising strategy for crack self-healing. Front Microbiol. 2015;6: 1–14.
[72] Mignon A, Snoeck D, D'Halluin K, et al. Alginate biopolymers: Counteracting the impact of superabsorbent polymers on mortar strength. Constr Build Mater. 2016;110:169–174.
[73] Aday AN, Osio-Norgaard J, Foster KEO, et al. Carrageenan-based superabsorbent biopolymers mitigate autogenous shrinkage in ordinary Portland cement. Mater Struct. 2018;51(2):37.
[74] Aday AN, Srubar WV. Biobased polymers for mitigating early- and late-age cracking in concrete. In: Bio-Based Materials and Biotechnologies for Eco-Efficient Construction. Cambridge, England: Woodhead Publishing; 2020. p. 19–41.
[75] Snoeck D, Moerkerke B, Mignon A, et al. In-situ crosslinking of superabsorbent polymers as external

curing layer compared to internal curing to mitigate plastic shrinkage. Constr Build Mater. 2020;262: 120819.
[76] Mignon A, Devisscher D, Graulus G-J, et al. Combinatory approach of methacrylated alginate and acid monomers for concrete applications. Carbohydr Polym. 2017;155:448–455.
[77] Snoeck D, Dubruel P, De Belie N. How to seal and heal in cementitious materials by using superabsorbent polymers cracks. In: Mechtcherine V, Schröfl C, editors. Proc pro 95 Int RILEM conf appl superabsorbent polym other new admixtures concr constr. France: RILEM publications S.A.R.L.; 2014. p. 375–384.
[78] Markovic M, Van Hoorick J, Hölzl K, et al. Hybrid tissue engineering scaffolds by combination of three-dimensional printing and cell photoencapsulation. J Nanotechnol Eng Med. 2015;6:210011–210017.
[79] Molnar K, Juriga D, Nagy PM, et al. Electrospun poly(aspartic acid) gel scaffolds for artificial extracellular matrix. Polym Int. 2014;63(9):1608–1615.
[80] Németh C, Szabó D, Gyarmati B, et al. Effect of side groups on the properties of cationic polyaspartamides. Eur Polym J. 2017;93:805–814.
[81] Snoeck D, Schröfl C, Mechtcherine V. Recommendation of RILEM TC 260-RSC: testing sorption by superabsorbent polymers (SAP) prior to implementation in cement-based materials. Mater Struct. 2018;51(5):116.
[82] Snoeck D, Schaubroeck D, Dubruel P, et al. Effect of high amounts of superabsorbent polymers and additional water on the workability, microstructure and strength of mortars with a water-to-cement ratio of 0.50. Constr Build Mater. 2014;72:148–157.
[83] Jakobsen UH, Pade C, Thaulow N, et al. Automated air void analysis of hardened concrete — a Round Robin study. Cem Concr Res. 2006;36(8):1444–1452.
[84] Liao W-C, Chen P-S, Hung C-W, et al. An innovative test method for tensile strength of concrete by applying the strut-and-Tie methodology. Materials (Basel). 2020;13(12):2776.
[85] Van Mullem T. Development of standard testing methods to evaluate the self-healing efficiency of concrete. Ghent, Belgium: Ghent University; 2021.
[86] Shin KJ, Bae W, Choi S-W, et al. Parameters influencing water permeability coefficient of cracked concrete specimens. Constr Build Mater. 2017;151:907–915.
[87] Sandoval GFB, Galobardes I, Teixeira RS, et al. Comparison between the falling head and the constant head permeability tests to assess the permeability coefficient of sustainable pervious concretes. Case Stud Constr Mater. 2017;7:317–328.
[88] Van Hoorick J, Gruber P, Markovic M, et al. Highly reactive thiol-norbornene photo-click hydrogels: toward improved processability. Macromol. Rapid Commun. 2018;39(14):1800181.
[89] Lin C-C, Ki CS, Shih H. Thiol-norbornene photoclick hydrogels for tissue engineering applications. J Appl Polym Sci. 2015;132:41563.
[90] Chiou B-S, English RJ, Khan SA. Rheology and photocross-linking of thiol – ene polymers. Macromolecules. 1996;29(16):5368–5374.
[91] Yang L, Li Y, Qian B, et al. Polyaspartic acid as a corrosion inhibitor for WE43 magnesium alloy. J Magnes Alloy. 2015;3(1):47–51.
[92] Andersson K, Allard B, Bengtsson M, et al. Chemical composition of cement pore solutions. Cem Concr Res. 1989;19(3):327–332.
[93] Kang S-H, Hong S-G, Moon J. Importance of monovalent ions on water retention capacity of superabsorbent polymer in cement-based solutions. Cem Concr Compos. 2018;88:64–72.
[94] Hancock RD, Martell AE. Ligand design for selective complexation of metal ions in aqueous solution. Chem Rev. 1989;89(8):1875–1914.
[95] Lee HXD, Wong HS, Buenfeld NR. Effect of alkalinity and calcium concentration of pore solution on the swelling and ionic exchange of superabsorbent polymers in cement paste. Cem Concr Compos. 2018;88: 150–164.
[96] Van Der Putten J, Snoeck D, De Coensel R, et al. Early age shrinkage phenomena of 3D printed cementitious materials with superabsorbent polymers. J Build Eng. 2021;35:102059.
[97] Laustsen S, Hasholt MT, Jensen OM. Void structure of concrete with superabsorbent polymers and its relation to frost resistance of concrete. Mater Struct. 2015; 48(1–2):357–368.
[98] Mignon A, Snoeck D, Schaubroeck D, et al. pH-responsive superabsorbent polymers: a pathway to self-healing of mortar. React Funct Polym. 2015;93:68–76.
[99] Hasholt MT, Jensen OM, Kovler K, et al. Can superabsorent polymers mitigate autogenous shrinkage of internally cured concrete without compromising the strength? Constr Build Mater. 2012;31:226–230.
[100] Snoeck D. Self-healing and microstructure of cementitious materials with microfibres and superabsorbent polymers. Ghent, Belgium: Ghent University; 2015.
[101] Snoeck D, Pel L, De Belie N. Autogenous healing in cementitious materials with superabsorbent polymers quantified by means of NMR. Sci Rep. 2020;10(1):642.
[102] Van Tittelboom K, De Belie N. Self-healing in cementitious materials—A review. Materials (Basel). 2013; 6(6):2182–2217.
[103] Rimshin V, Truntov P. Determination of carbonation degree of existing reinforced concrete structures and their restoration. E3S Web Conf. 2019;135:03015. Rudoy D, Murgul V, editors.
[104] Lo Y, Lee HM. Curing effects on carbonation of concrete using a phenolphthalein indicator and fourier-transform infrared spectroscopy. Build Environ. 2002; 37(5):507–514.
[105] Chang C-F, Chen J-W. The experimental investigation of concrete carbonation depth. Cem Concr Res. 2006; 36(9):1760–1767.
[106] von Greve-Dierfeld S, Lothenbach B, Vollpracht A, et al. Understanding the carbonation of concrete with supplementary cementitious materials: a critical review by RILEM TC 281-CCC. Mater Struct. 2020;53(6):136.
[107] Snoeck D, Roigé N, Manso S, et al. The effect of (and the potential of recycled) superabsorbent polymers on the water retention capability and bio-receptivity of cementitious materials. Resour Conserv Recycl. 2022;177:106016.